



Supplement of

Spatially and temporally resolved ice loss in High Mountain Asia and the Gulf of Alaska observed by CryoSat-2 swath altimetry between 2010 and 2019

Livia Jakob et al.

Correspondence to: Livia Jakob (livia@earthwave.co.uk)

The copyright of individual parts of the supplement might differ from the article licence.

Supplementary Information

for

Spatially and temporally resolved ice loss in High Mountain Asia and the Gulf of Alaska observed by CryoSat-2 swath altimetry between 2010 and 2019

Livia Jakob, Noel Gourmelen, Martin Ewart, Stephen Plummer

Here we provide supplementary information about:

- 10 - Quality thresholds used for data processing
- Handling of missing data
- Uncertainty assessment
- Supplementary figures and tables

1 Supplementary information about data processing and methodology

15 1.1 Quality weights for dh/dt

When generating time-dependent elevation changes we use weights, based on attributes (power and coherence) to penalise lower quality measurements. We use the following formula to calculate a quality rating (see Gourmelen et al., 2018),

$$w_v = \frac{v^2}{\max (v_{i=1}^n)^2}, \quad (1)$$

where v is an attribute value (either power or coherence) and w_v the attribute weight rating. We then average the weight ratings to retrieve a single quality weight for each measurement.

1.2 Quality for dh/dt bins

We remove 100 x 100 km bins that exceed a set of quality criteria. As described in the corresponding paper we calculate a 30-day surface elevation time series for each bin, which is used as an additional check of the dh/dt quality of a bin (note that the rate of change of each bin is calculated fitting a trend to all the $elevDiff$ ¹ measurements and not based on the time series). To remove low quality bins from the results we define a set of minimal thresholds:

¹ $elevDiff$ describes the elevation differences between the TanDEM-X 90m DEM (German Aerospace Center [DLR], 2018) and the swath elevation measurements, i.e. topography is removed.

- (1) Elevation change uncertainties: Bins with uncertainties higher than 1 m yr^{-1} are excluded.
- (2) Temporal completeness: We used the degree of completeness of the corresponding time series to exclude bins with a number of 30-day periods that did not show any measurements. Bins with less than 60% temporal coverage were excluded.
- 30 (3) Interannual change: The standard deviation of the corresponding time series (with the rate removed) was used to exclude bins with unrealistically high interannual change. Bins with a standard deviation higher than 10 were excluded.
- (4) Stability of regression results: We use the spread of results from different regression models (using a set of different quality weightings and outlier removal approaches), as a means of identifying grid cells where the results are particularly sensitive to data sampling, data distribution and quality weightings. Bins with a standard error of the
35 mean of a set of regression results larger than 0.15 m yr^{-1} have been excluded.

1.3 Filling gaps with hypsometric averaging

Our hypsometric model makes use of the relation between elevation and dh/dt to extrapolate rates of elevation change (Moholdt et al., 2010a, 2010b; Nilsson et al., 2015). For each sub-region we calculate time-dependent rates of elevation changes in 100m
40 elevation bands. We use the RGI 6.0 second order regions (RGI Consortium, 2017), containing sub-regions sufficiently large to retrieve enough measurements per elevation band. We fit one to three order polynomials to the relation between elevation and dh/dt , where the order of the polynomial was decided based on iterative increase of the polynomial order until the adjusted R^2 coefficient stabilised (Nilsson et al., 2015). In addition, subjective judgement was used to avoid runaway tails (Nuth et al., 2010). The elevation dependent dh/dt curves, fitted polynomials and hypsometry functions for each sub-region are shown in
45 Figure 6 and Figure 11 in the paper.

For each 100 m elevation band k we calculate the rate of change $\Delta h(k)$ based on the fitted polynomials and multiply it with the glacierised area of the band $A(k)$ to extract volume change $V(k)$. $A(k)$ is retrieved for each elevation band using the TanDEM-X DEM and the RGI 6.0 glacier masks. The sum of all $V(k)$ represents the total volume change rate in a bin or region.

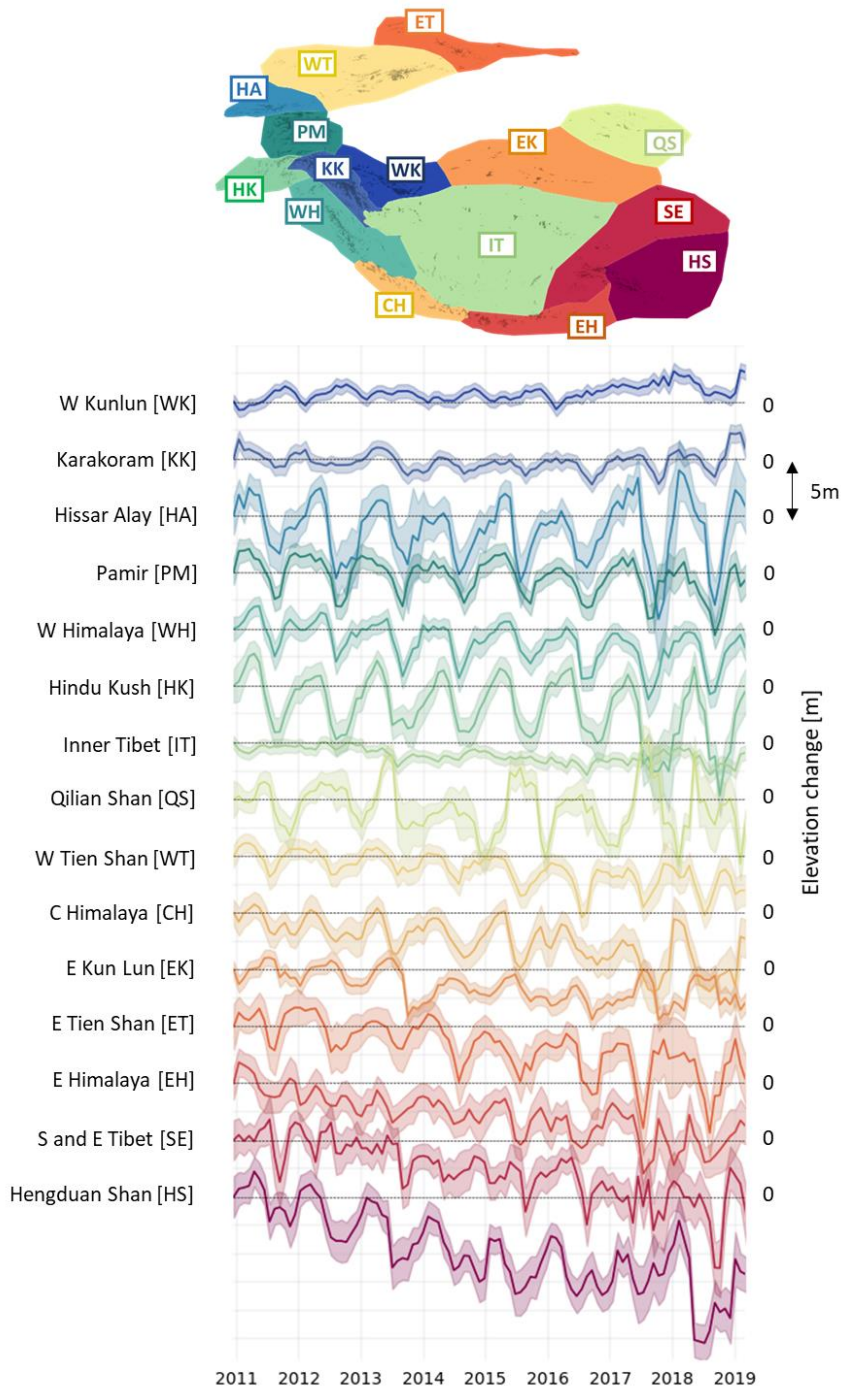
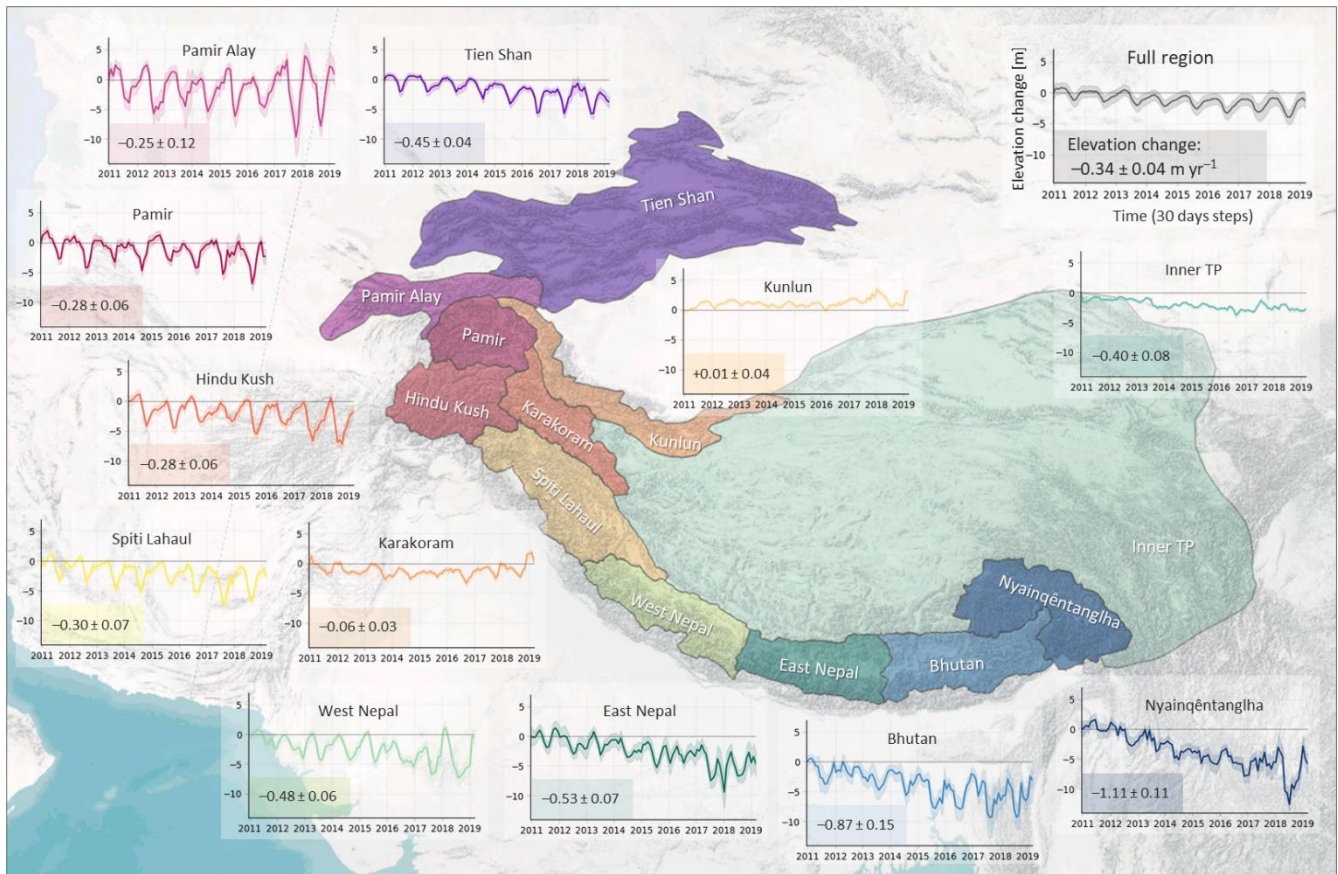
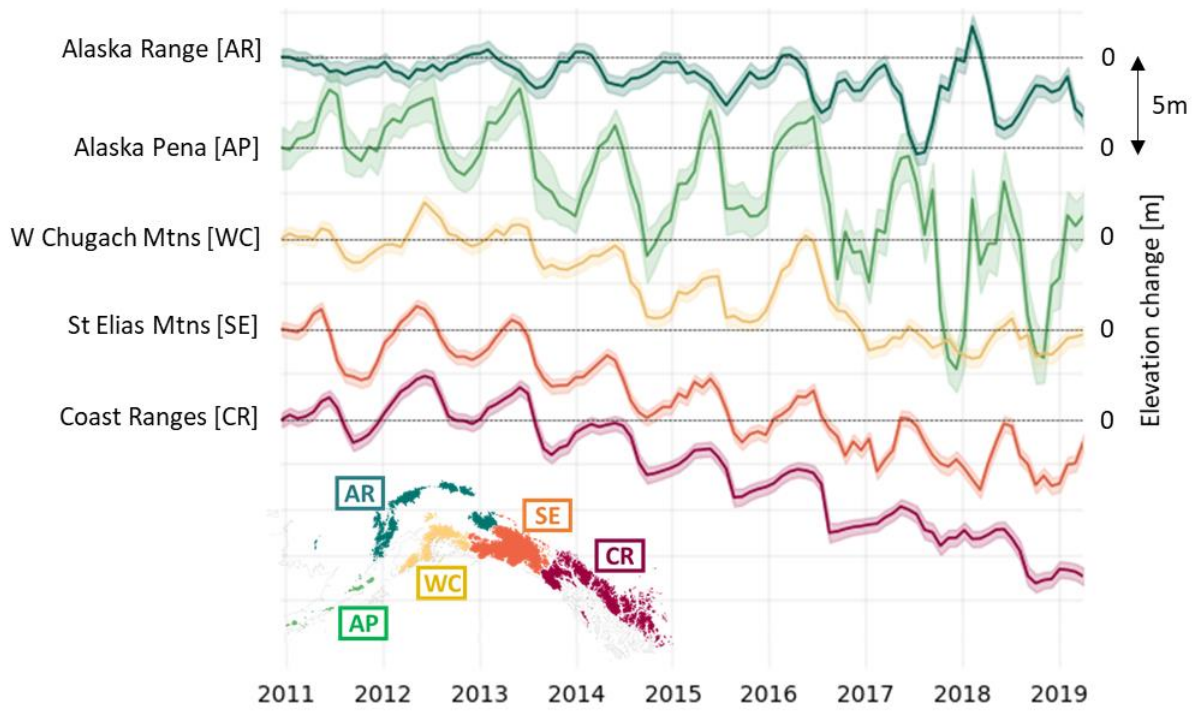


Figure S1: High Mountain Asia (HMA) monthly elevation change time series with uncertainty envelopes on sub-regional level (RGI second order regions) sorted by rate of elevation change.



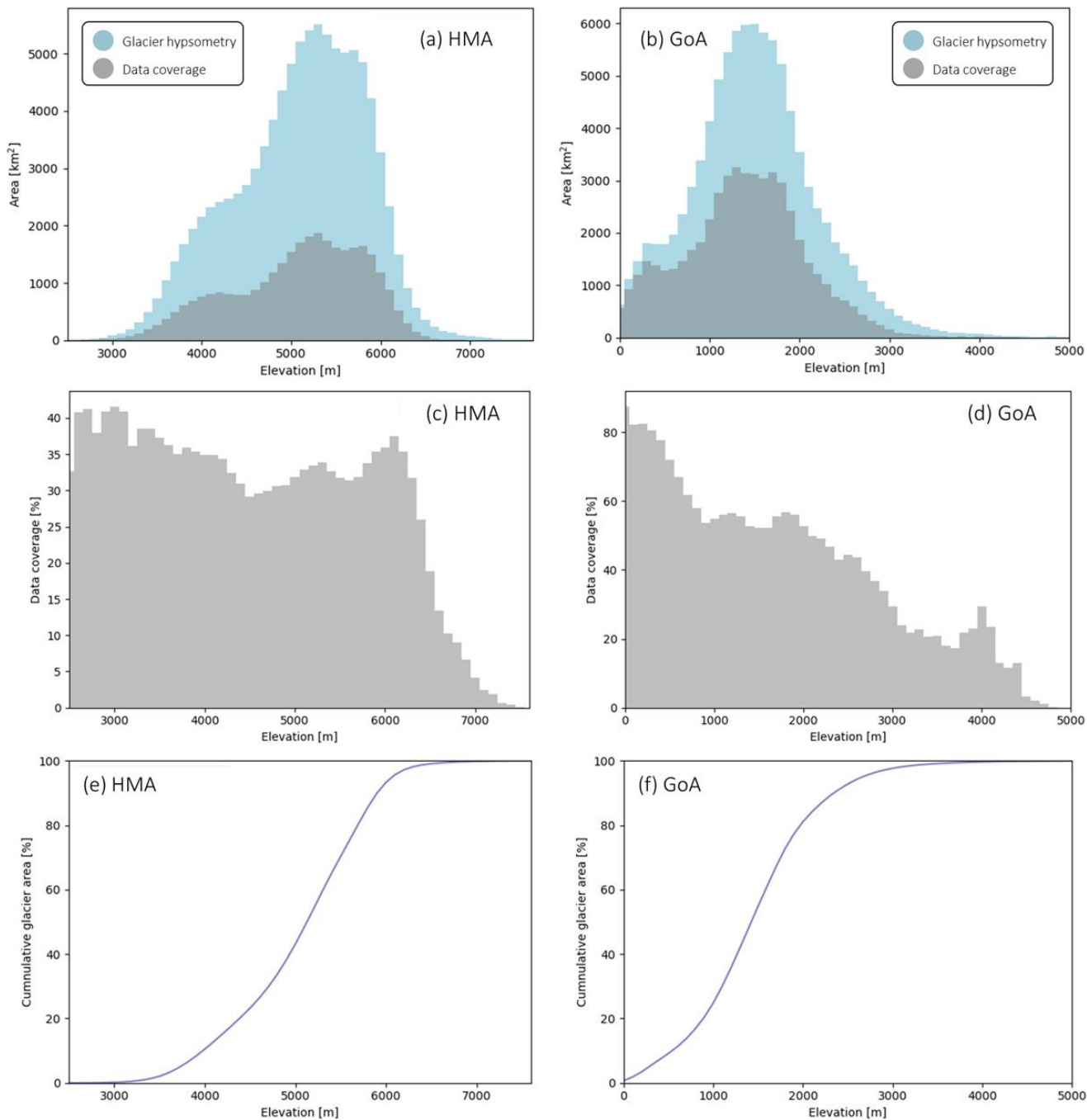
55

Figure S2: High Mountain Asia (HMA) 30-day elevation change time series on a sub-regional level using the mask by Brun et al. (2017). The coloured lines display the time series with the uncertainty envelope (y-axis: elevation change [m], x-axis: time [30-days steps]). The numbers describe the elevation change with uncertainties in m yr⁻¹.

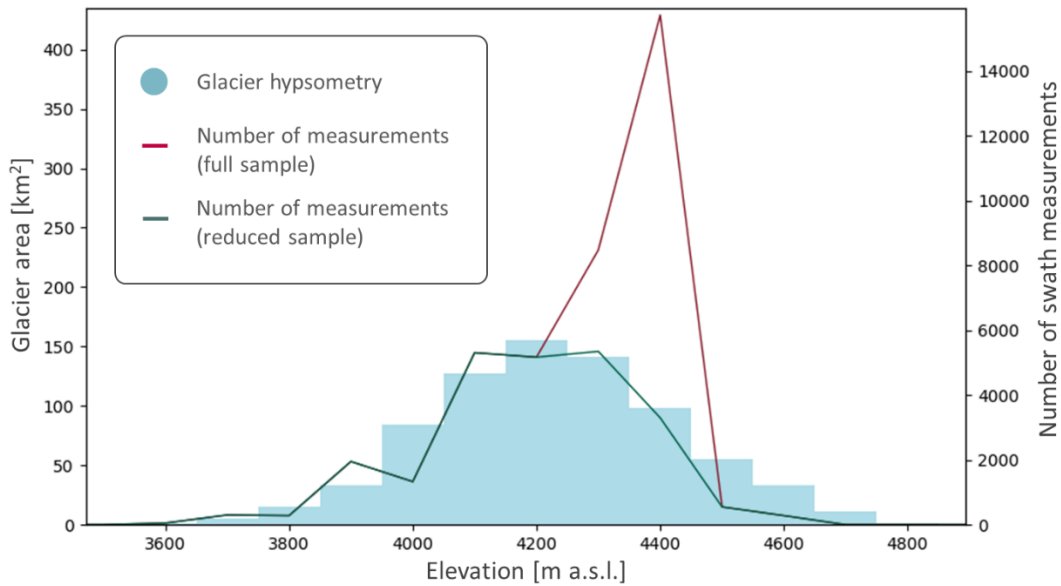


60

Figure S3: Gulf of Alaska (GoA) monthly elevation change time series on sub-regional level (RGI 6.0 second order regions) sorted by rate of elevation change.

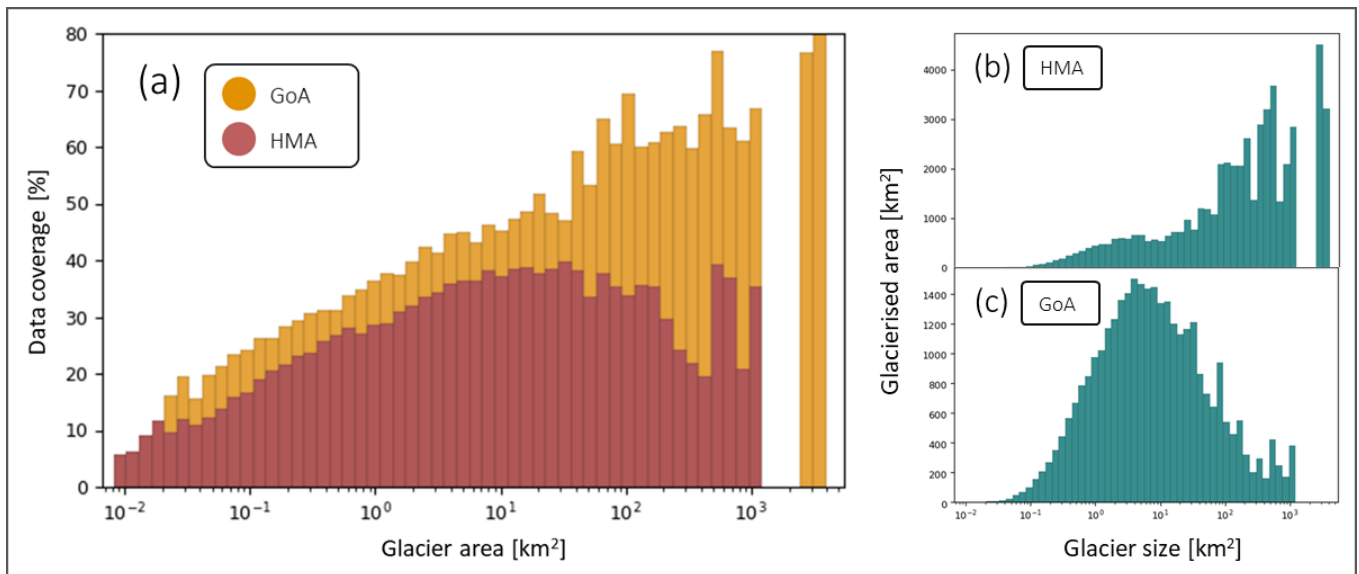


65 **Figure S4:** Figure (a) and (b) display glacier hypsometry (light blue) and swath elevation data coverage (grey) for the two regions High Mountain Asia (a) and the Gulf of Alaska (b). Figure (c) and (d) display data coverage as a percentage of the glacier hypsometry and figure (e) and (f) display the cumulative glacier area.



70 **Figure S5: Illustration of elevation bias removal by sub-sampling for an example 100 x 100 km bin in High Mountain Asia. The light blue bars represent the glacier hypsometry within the bin (*y-axis, left*) and the red line (*y-axis, right*) displays the number of swath measurement of the full sample showing a bias towards higher elevations. After sequentially removing swath measurements based on measurement uncertainty to match the glacier hypsometry (using a 5% threshold) we achieve the swath elevation measurements distribution displayed as the green line (*y-axis, right*). This procedure reduces potential biases in the altitudinal distribution of observations but also leads to a sample reduction.**

75



80 **Figure S6: Relation between glacier size and CryoSat-2 swath elevation data coverage in High Mountain Asia and the Gulf of Alaska region (a), hypsometry of glacier sizes in the Gulf of Alaska (b) and in High Mountain Asia (c). For High Mountain Asia we achieve a data coverage of 25% for glaciers smaller than 1 km² (representing 21% of total glaciersised area), 34% coverage for glaciers between 1 and 10 km² (representing 39% of total glaciersised area), 37% coverage for glaciers between 10 and 100 km² (representing**

28% of total glacierised area) and 31% coverage for glaciers larger than 100 km² (representing 12% of total glacierised area). For the Gulf of Alaska we achieve a coverage of 31% for glaciers smaller than 1 km² (representing 8% of total glacierised area), 42% coverage for glaciers between 1 and 10 km² (representing 15% of total glacierised area), 54% coverage for glaciers between 10 and 100 km² (representing 21% of total glacierised area) and 68% coverage for glaciers larger than 100 km² (representing 56% of total glacierised area).

85

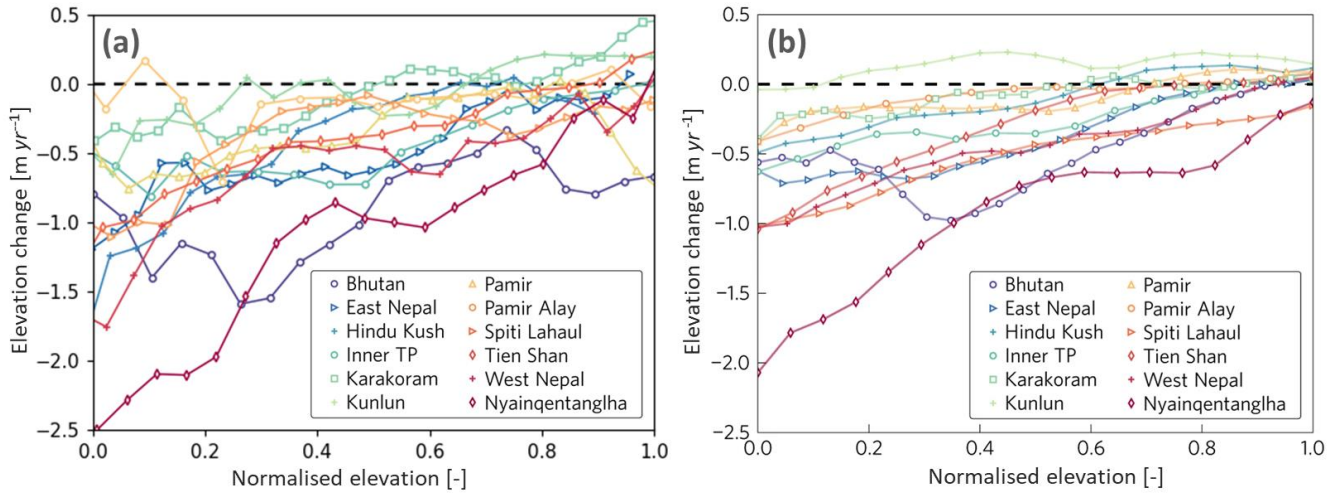
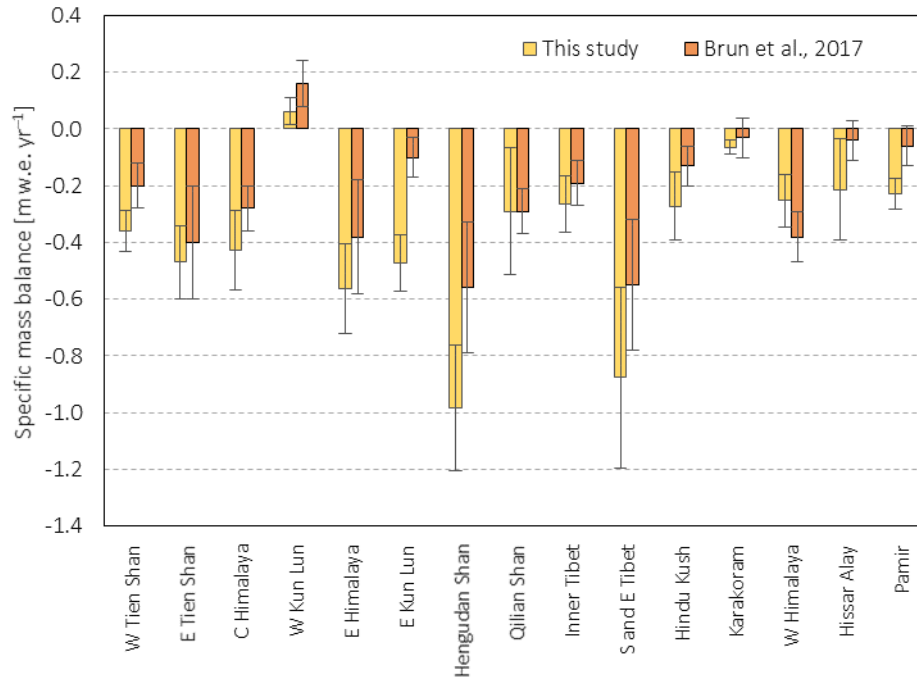


Figure S7: Elevation change rates in HMA (in 100 m elevation bins) as a function of normalised elevation from this study (a) in comparison with Brun et al. (2017) (b). To normalise elevation the formula $(z - z_{2.5}) / (z_{97.5} - z_{2.5})$ is used, with z as elevation and $z_{2.5}$ as the elevation at 2.5 percentile of glacierised area and $z_{97.5}$ as the elevation at 97.5 percentile of glacierised area.

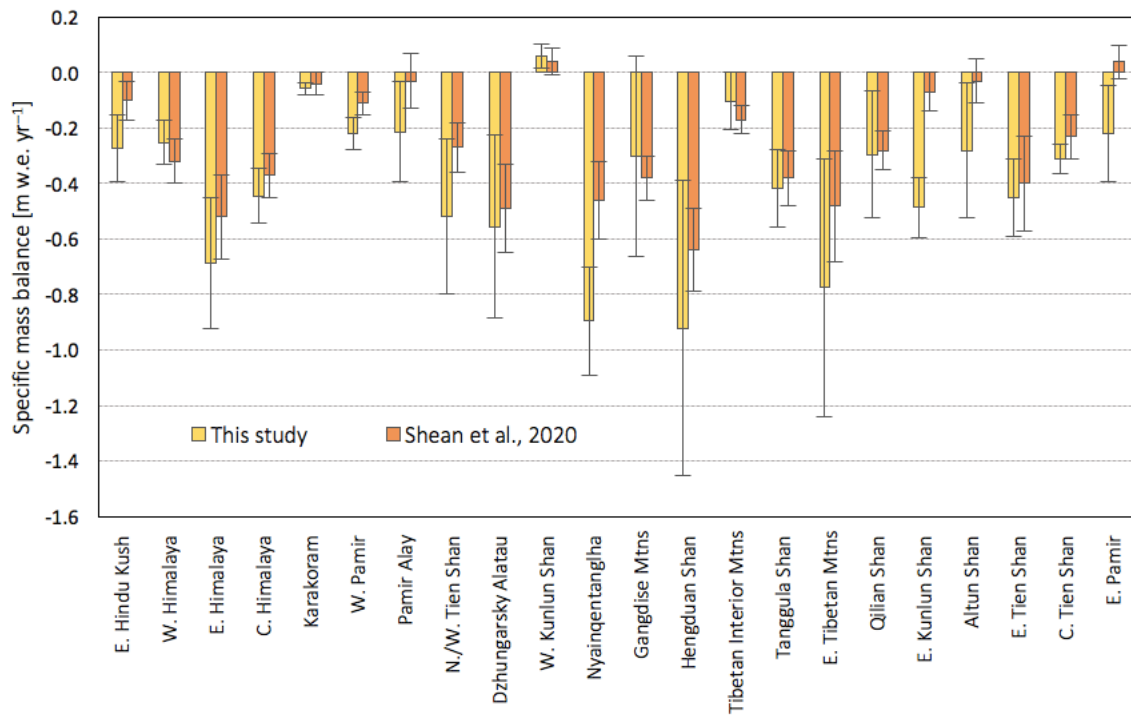
90

95



100

Figure S8: High Mountain Asia (HMA) specific mass balance trends on a sub-regional level (using the RGI 6.0 second order sub-regions) in comparison with Brun et al. (2017). This study covers the time period of 2010 to 2019, whilst Brun et al. (2017) cover the time period of 2000 to 2016.



105

Figure S9: High Mountain Asia (HMA) specific mass balance trends on a sub-regional level (using the HiMAP sub-regions) in comparison with Shean et al. (2020). This study covers the time period of 2010 to 2019, whilst Shean et al. (2020) cover the time period of 2000 to 2018.

110

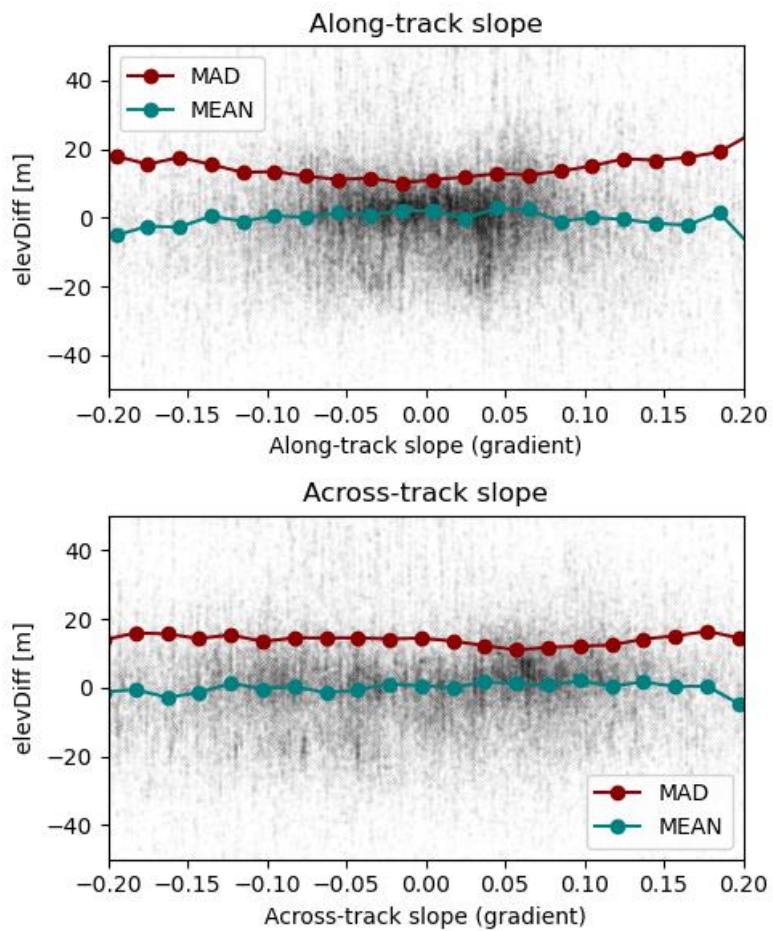


Figure S10: Differences between the TanDEM-X 90m DEM (German Aerospace Center [DLR], 2018) and the swath elevation measurements in Hissar Alay for different along-track and across-track slopes, including median average deviation (MAD) and mean (MEAN) of the elevation differences (referred to as *elevDiff*).

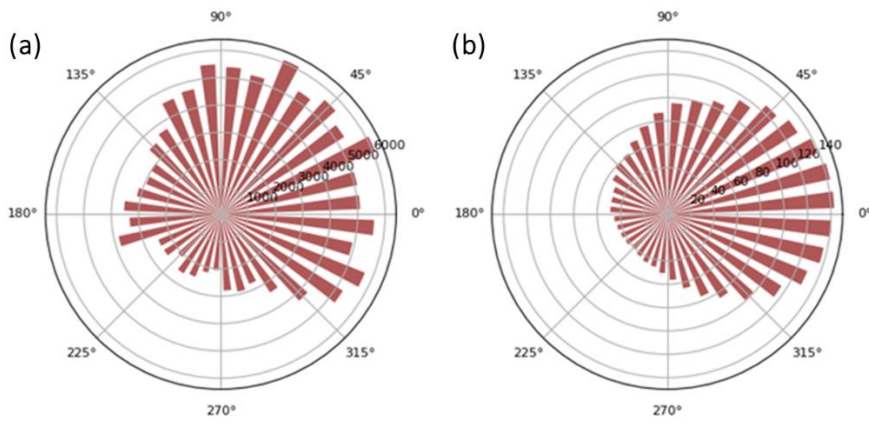


Figure S11: Distribution of aspect in our swath elevation measurements (a) and the distribution of glacier aspects (b) in Hissar Alay.

3 Supplementary tables

	Glacier area [km ²]	This study [m w.e. yr ⁻¹]	Shean et al., 2020 [m w.e. yr ⁻¹]	Brun et al., 2017 [m w.e. yr ⁻¹]	Kääb et al., 2015 [m w.e. yr ⁻¹]
Inner TP	13537	-0.34 ± 0.09	-0.22 ± 0.05	-0.14 ± 0.07	-0.06 ± 0.06
Kunlun	10420	+0.01 ± 0.05	+0.04 ± 0.04	+0.14 ± 0.08	+0.18 ± 0.14
Pamir Alay	1917	-0.22 ± 0.22	-0.04 ± 0.09	-0.04 ± 0.00	-0.59 ± 0.27
Nyainqêntanglha	6944	-0.95 ± 0.19	-0.50 ± 0.15	-0.62 ± 0.23	-1.14 ± 0.58
East Nepal (Everest)	4980	-0.45 ± 0.14	-0.36 ± 0.09	-0.33 ± 0.20	-0.31 ± 0.14
Bhutan	2355	-0.74 ± 0.28	-0.55 ± 0.17	-0.42 ± 0.20	-0.76 ± 0.20
West Nepal	4657	-0.41 ± 0.16	-0.37 ± 0.09	-0.34 ± 0.09	-0.37 ± 0.15
Karakoram	20234	-0.05 ± 0.03	-0.04 ± 0.04	-0.03 ± 0.07	-0.09 ± 0.12
Spiti-Lahaul	7746	-0.26 ± 0.08	-0.31 ± 0.08	-0.37 ± 0.09	-0.42 ± 0.26
Pamir	7095	-0.24 ± 0.06	-0.11 ± 0.04	-0.08 ± 0.07	-0.41 ± 0.24
Hindu Kush	5326	-0.23 ± 0.08	-0.09 ± 0.06	-0.12 ± 0.07	-0.42 ± 0.18
Tien Shan	12099	-0.38 ± 0.06	-0.29 ± 0.07	-0.28 ± 0.20	-0.37 ± 0.31
Total	97310				

Table S1: High Mountain Asia (HMA) specific mass balance trends on a sub-regional level in comparison with DEM differencing and ICESat studies. It is important to note that Shean et al. (2020) cover the time period of 2000 to 2018, Brun et al. (2017) cover the time period of 2000 to 2016 and Kääb et al. (2015) cover the time period 2003 to 2008, whilst this study covers the time period of 2010 to 2019. We have complemented the data from Kääb et al. (2015) with ICESat data from Brun et al. (2017) for the sub-regions Kunlun, Inner TP, Tien Shan and Pamir Alay, which extended the estimates of Kääb et al. (2015) using the same method.

125

	Glacier area [km ²]	Specific mass change [m w.e. yr ⁻¹]	Mass change [Gt yr ⁻¹]
Eastern Hindu Kush	2938	-0.27 ± 0.12	-0.79 ± 0.35
Western Himalaya	7986	-0.25 ± 0.08	-2.00 ± 0.64
Eastern Himalaya	2844	-0.69 ± 0.24	-1.94 ± 0.67
Central Himalaya	8682	-0.44 ± 0.10	-3.84 ± 0.86
Karakoram	21472	-0.06 ± 0.02	-1.25 ± 0.49
Western Pamir	8418	-0.22 ± 0.06	-1.85 ± 0.48
Pamir Alay	1846	-0.21 ± 0.18	-0.39 ± 0.33
Northern/Western Tien Shan	2261	-0.52 ± 0.28	-1.17 ± 0.63
Dzhungarsky Alatau	521	-0.56 ± 0.33	-0.29 ± 0.17
Western Kunlun Shan	8457	+0.06 ± 0.04	+0.51 ± 0.38
Nyainqêntanglha	7047	-0.89 ± 0.19	-6.29 ± 1.37
Gangdise Mountains	1271	-0.30 ± 0.36	-0.38 ± 0.46
Hengduan Shan	1282	-0.92 ± 0.53	-1.18 ± 0.68

Tibetan Interior Mountains	3815	-0.10 ± 0.10	-0.39 ± 0.39
Tanggula Shan	1841	-0.42 ± 0.14	-0.77 ± 0.26
Eastern Tibetan Mountains	312	-0.78 ± 0.46	-0.24 ± 0.14
Qilian Shan	1598	-0.30 ± 0.23	-0.47 ± 0.36
Eastern Kunlun Shan	2995	-0.49 ± 0.11	-1.45 ± 0.32
Altun Shan	295	-0.28 ± 0.24	-0.08 ± 0.07
Eastern Tien Shan	2333	-0.45 ± 0.14	-1.05 ± 0.32
Central Tien Shan	7270	-0.31 ± 0.05	-2.25 ± 0.39
Eastern Pamir	2118	-0.22 ± 0.17	-0.46 ± 0.37

Table S2: High Mountain Asia (HMA) mass balance trends from 2010 to 2019, aggregated on the HiMAP sub- regions (Bolch et al., 2019).

130

	d	c	b	a	d_{err}	c_{err}	b_{err}
Alaska Range (Wrangell/Kilbuck)	-3.008926357	0.001859164	-2.40E-07	0	0.020969151	-0.000015343	3.43E-09
Alaska Pena (Aleutians)	-6.293731373	0.010054900	-5.09E-06	8.01E-10	0.086787480	-0.000181579	9.20E-08
West Chugach Mountains (Talkeetna)	-4.678348693	0.004822413	-1.67E-06	1.95E-10	0.013348888	-0.000017687	6.00E-09
Saint Elias Mountains	-3.463044478	0.002119418	-3.19E-07	0	0.011000255	-0.000016267	4.88E-09
Northern Coast Ranges	-3.224674716	0.001212905	0	0	0.016748088	-0.00002028	6.24E-09

Table S3: Polynomial coefficients describing the altitudinal distribution of elevation change rates $\sigma_{\Delta h}(k)$ and their corresponding errors $\sigma_{\Delta h, err}(k)$ in the Alaska RGI 6.0 second order regions calculated from CryoSat-2 swath elevations between 2010 and 2019. Elevation changes in relation to altitude [m yr⁻¹] are described as one to three order polynomials $\sigma_{\Delta h}(k) = ak^3 + bk^2 + ck + d$ and the corresponding errors [m yr⁻¹] are described as two order polynomials $\sigma_{\Delta h, err}(k) = b_{err}k^2 + c_{err}k + d$ with k representing the elevation in m a.s.l.

135

	d	c	b	a	d_{err}	c_{err}	b_{err}
W Tien Shan	-5.430894095	0.001733559	-1.27E-07	0	0.720746599	-0.000317986	3.52E-08
E Tien Shan	17.85412608	-0.015099888	3.83E-06	-3.00E-10	2.319628442	-0.001166496	1.47E-07
C Himalaya	-69.60125902	0.037561058	-6.87E-06	4.23E-10	1.262957906	-0.000455633	4.12E-08
W Kun Lun	-2.139410906	0.000369918	0	0	1.270803238	-0.000422618	3.51E-08
E Himalaya	5.85068851	-0.002646660	2.62E-07	0	1.480776241	-0.000493023	4.13E-08
E Kun Lun	24.04975963	-0.010042428	1.01E-06	0	3.657901747	-0.00129725	1.15E-07
Hengduan Shan	22.94585098	-0.018957305	4.50E-06	-3.33E-10	2.319262315	-0.000949568	9.75E-08
Qilian Shan	75.33063669	-0.047931962	9.89E-06	-6.65E-10	6.115713322	-0.002381989	2.32E-07
Inner Tibet	-36.98988913	0.011858705	-9.51E-07	0	4.028370667	-0.001358846	1.14E-07
S and E Tibet	-11.77499997	0.003139844	-2.01E-07	0	0.248414888	-0.000068618	4.89E-09
Hindu Kush	-45.56736806	0.025203846	-4.78E-06	3.10E-10	2.194926188	-0.000874117	8.72E-08
Karakoram	-0.242945069	-0.000234290	5.03E-08	0	0.170047737	-0.000064542	6.37E-09
W Himalaya	-2.081792054	0.000335344	0	0	0.825667399	-0.000298594	2.71E-08
Hissar Alay	-0.608265349	0.000113994	0	0	1.228736870	-0.000578951	6.90E-08
Pamir	51.55194542	-0.035473036	7.90E-06	-5.73E-10	0.439495691	-0.000176018	1.80E-08

140

Table S4: Polynomial coefficients describing the altitudinal distribution of elevation change rates $\sigma_{\Delta h}(k)$ and their corresponding errors $\sigma_{\Delta h, err}(k)$ in the High Mountain Asia RGI 6.0 second order regions calculated from CryoSat-2 swath elevations between 2010 and 2019. Elevation changes in relation to altitude [m yr⁻¹] are described as one to three order polynomials $\sigma_{\Delta h}(k) = ak^3 + bk^2 + ck + d$ and the corresponding errors [m yr⁻¹] are described as two order polynomials $\sigma_{\Delta h, err}(k) = b_{err}k^2 + c_{err}k + d$ with k representing the elevation in m a.s.l.

- Berthier, E., Schiefer, E., Clarke, G. K. C., Menounos, B. and Rémy, F.: Contribution of Alaskan glaciers to sea-level rise derived from satellite imagery, *Nat. Geosci.*, 3(2), 92–95, doi:10.1038/ngeo737, 2010.
- Berthier, E., Vincent, C., Magnússon, E., Gunnlaugsson, Á. P., Pitte, P., Le Meur, E., Masiokas, M., Ruiz, L., Pálsson, F., Belart, J. M. C. and Wagnon, P.: Glacier topography and elevation changes derived from Pléiades sub-meter stereo images, *The Cryosphere*, 8(6), 2275–2291, doi:10.5194/tc-8-2275-2014, 2014.
- Bolch, T., Shea, J. M., Liu, S., Azam, F. M., Gao, Y., Gruber, S., Immerzeel, W. W., Kulkarni, A., Li, H., Tahir, A. A., Zhang, G. and Zhang, Y.: Status and Change of the Cryosphere in the Extended Hindu Kush Himalaya Region, in *The Hindu Kush Himalaya Assessment: Mountains, Climate Change, Sustainability and People*, edited by P. Wester, A. Mishra, A. Mukherji, and A. B. Shrestha, pp. 209–255, Springer International Publishing, Cham., 2019.
- 155 Brun, F., Berthier, E., Wagnon, P., Kääb, A. and Treichler, D.: A spatially resolved estimate of High Mountain Asia glacier mass balances from 2000 to 2016, *Nat. Geosci.*, 10(9), 668–673, doi:10.1038/ngeo2999, 2017.
- German Aerospace Center (DLR): TanDEM-X - Digital Elevation Model (DEM) - Global, 90m, , doi:10.15489/ju28hc7pui09, 2018.
- Gourmelen, N., Escorihuela, M., Shepherd, A., Foresta, L., Muir, A., Garcia-Mondejar, A., Roca, M., Baker, S. and Drinkwater, M. R.: CryoSat-2 swath interferometric altimetry for mapping ice elevation and elevation change, *Adv. Space Res.*, doi:10.1016/j.asr.2017.11.014, 2018.
- Huss, M.: Density assumptions for converting geodetic glacier volume change to mass change, *The Cryosphere*, 7(3), 877–887, doi:10.5194/tc-7-877-2013, 2013.
- Moholdt, G., Hagen, J. O., Eiken, T. and Schuler, T. V.: Geometric changes and mass balance of the Austfonna ice cap, Svalbard, *The Cryosphere*, 4(1), 21–34, doi:10.5194/tc-4-21-2010, 2010a.
- 165 Moholdt, G., Nuth, C., Hagen, J. O. and Kohler, J.: Recent elevation changes of Svalbard glaciers derived from repeat track ICESat altimetry, *Remote Sens. Environ.*, 114(11), 2756–2767, doi:10.1016/j.rse.2010.06.008, 2010b.
- Nilsson, J., Sandberg Sørensen, L., Barletta, V. R. and Forsberg, R.: Mass changes in Arctic ice caps and glaciers: implications of regionalizing elevation changes, *The Cryosphere*, 9(1), 139–150, doi:10.5194/tc-9-139-2015, 2015.
- 170 Nuth, C., Moholdt, G., Kohler, J., Hagen, J. O. and Kääb, A.: Svalbard glacier elevation changes and contribution to sea level rise, *J. Geophys. Res. Earth Surf.*, 115(F1), doi:10.1029/2008JF001223, 2010.
- Pfeffer, W. T., Arendt, A. A., Bliss, A., Bolch, T., Cogley, J. G., Gardner, A. S., Hagen, J.-O., Hock, R., Kaser, G., Kienholz, C., Miles, E. S., Moholdt, G., Mölg, N., Paul, F., Radić, V., Rastner, P., Raup, B. H., Rich, J., Sharp, M. J. and Consortium, T. R.: The Randolph Glacier Inventory: a globally complete inventory of glaciers, *J. Glaciol.*, 60(221), 537–552, doi:10.3189/2014JG13J176, 2014.
- 175 RGI Consortium: Randolph Glacier Inventory – A Dataset of Global Glacier Outlines: Version 6.0, Technical Report, Global Land Ice Measurements from Space, Digit. Media, doi:10.7265/N5-RGI-60, 2017.
- Shean, D. E., Bhushan, S., Montesano, P., Rounce, D. R., Arendt, A. and Osmanoglu, B.: A Systematic, Regional Assessment of High Mountain Asia Glacier Mass Balance, *Front. Earth Sci.*, 7, doi:10.3389/feart.2019.00363, 2020.

